

Southern Hemisphere Cloud–Dynamics Biases in CMIP5 Models and Their Implications for Climate Projections

KEVIN M. GRISE

Lamont-Doherty Earth Observatory, Columbia University, Palisades, New York

LORENZO M. POLVANI

Lamont-Doherty Earth Observatory, Department of Applied Physics and Applied Mathematics, and Department of Earth and Environmental Sciences, Columbia University, New York, New York

(Manuscript received 6 February 2014, in final form 5 May 2014)

ABSTRACT

This study quantifies cloud–radiative anomalies associated with interannual variability in the latitude of the Southern Hemisphere (SH) midlatitude eddy-driven jet, in 20 global climate models from phase 5 of the Coupled Model Intercomparison Project (CMIP5). Two distinct model types are found. In the first class of models (type I models), total cloud fraction is reduced at SH midlatitudes as the jet moves poleward, contributing to enhanced shortwave radiative warming. In the second class of models (type II models), this dynamically induced cloud radiative warming effect is largely absent. Type I and type II models have distinct deficiencies in their representation of observed Southern Ocean clouds, but comparison with two independent satellite datasets indicates that the cloud–dynamics behavior of type II models is more realistic.

Because the SH midlatitude jet shifts poleward in response to CO₂ forcing, the cloud–dynamics biases uncovered from interannual variability are directly relevant for climate change projections. In CMIP5 model experiments with abruptly quadrupled atmospheric CO₂ concentrations, the global-mean surface temperature initially warms more in type I models, even though their equilibrium climate sensitivity is not significantly larger. In type I models, this larger initial warming is linked to the rapid adjustment of the circulation and clouds to CO₂ forcing in the SH, where a nearly instantaneous poleward shift of the midlatitude jet is accompanied by a reduction in the reflection of solar radiation by clouds. In type II models, the SH jet also shifts rapidly poleward with CO₂ quadrupling, but it is not accompanied by cloud radiative warming anomalies, resulting in a smaller initial global-mean surface temperature warming.

1. Introduction

It is well known that one of the present challenges for climate models is providing an accurate representation of global cloud cover. Because essential cloud processes occur on much smaller scales than typical model resolution, they need to be parameterized. As a consequence, feedbacks involving clouds, particularly low clouds, are responsible for most of the spread in climate sensitivity across climate models (Soden and Held 2006; Webb et al. 2006; Dufresne and Bony 2008; Williams and Webb 2009; Webb et al. 2013).

Numerous studies have identified marine boundary layer clouds as the dominant source of uncertainty in model cloud feedbacks (Bony and Dufresne 2005; Medeiros et al. 2008; Williams and Webb 2009). Much attention has thus been paid to the role of low clouds over tropical and subtropical ocean basins, but the important role of low clouds over the Southern Ocean has also recently been noted. Trenberth and Fasullo (2010) demonstrated that many global climate models substantially underestimate cloud fraction and albedo over the Southern Ocean, and therefore have a large bias in absorbed shortwave radiation there. Because the Southern Ocean is almost entirely covered by clouds in the present-day climatology (e.g., Bromwich et al. 2012), any underestimate of this cloud cover by models might lead to spurious feedbacks in future climate scenarios (Trenberth and Fasullo 2010). Biases in Southern Ocean cloud cover in models have also been

Corresponding author address: Kevin M. Grise, Lamont-Doherty Earth Observatory, Columbia University, P.O. Box 1000, 61 Route 9W, Palisades, NY 10964-8000.
E-mail: kgrise@ldeo.columbia.edu

linked to biases in the latitude of the Southern Hemisphere (SH) midlatitude eddy-driven jet (Ceppi et al. 2012) and the presence of a double intertropical convergence zone (Hwang and Frierson 2013).

Southern Ocean cloud cover is intimately related to extratropical weather systems, and thus to the position of the SH storm track and the midlatitude eddy-driven jet. Consequently, if the jet moves poleward (either as a result of natural variability or anthropogenic forcing), one might expect there to be a notable change in cloud radiative processes. Indeed, using a single climate model, the Community Atmosphere Model version 3 (CAM3), Grise et al. (2013, hereafter G13) found that a poleward shift in the SH midlatitude jet resulted in a sizeable cloud-induced shortwave radiative warming effect on the SH, as the bulk of the clouds (and their attendant reflection of sunlight) shifted poleward with the jet. Similar connections between a jet-induced shortwave warming and clouds have also been proposed using satellite data (Bender et al. 2012). However, using CAM5 (a newer version of the same model used by G13), Kay et al. (2014, hereafter K14) found little connection between jet variability and cloud radiative processes over the Southern Ocean.

Thus, the relationship between SH jet variability and cloud radiative processes appears to be model dependent, and it is unclear how these different behaviors affect climate projections. The goal of this study is to clarify the connections among jet variability, cloud radiative processes, and model sensitivity. To do this, we examine 20 global climate models that participated in phase 5 of the Coupled Model Intercomparison Project (CMIP5). We find that there are two distinct categories of models: those that have a strong cloud-induced shortwave warming effect associated with a poleward SH jet shift (as in G13) and those that do not (as in K14). These distinct behaviors are tied to biases in the mean-state cloud climatology of the models and, as we show below, have direct implications for the global-mean surface temperature warming projected by the models in response to CO₂ forcing.

The paper is organized as follows. Section 2 describes the data and methods used in this study. Section 3 introduces the two categories of CMIP5 models, and section 4 compares the two classes of models to observations. Section 5 examines the implications of the varying model behavior for climate projections. Section 6 concludes with a summary of our findings.

2. Data and methods

a. Data

The primary data used in this study are the monthly-mean output from the global climate models that

participated in CMIP5 (Taylor et al. 2012), provided courtesy of the Program for Climate Model Diagnosis and Intercomparison at Lawrence Livermore National Laboratory. Here, we use data from 20 of the 23 models for which the values of equilibrium climate sensitivity were computed by Forster et al. (2013) (see Table 1). We have excluded one model [Flexible Global Ocean–Atmosphere–Land System Model gridpoint, second spectral version (FGOALS-s2)], for which the historical scenario integrations were not available, and two other models [Goddard Institute for Space Studies Model E2, coupled respectively with the Hybrid Coordinate Ocean Model (HYCOM) (GISS-E2-H) and the Russell ocean model (GISS-E2-R)], which fail to produce the observed large negative values of shortwave cloud radiative effect over the Southern Ocean; all other models were retained. For each of the models, we analyze three different forcing scenarios: 1) preindustrial control (i.e., hundreds of years of unforced variability), 2) historical (driven by 1850–2005 forcings), and 3) abrupt 4×CO₂ (in which atmospheric carbon dioxide is instantaneously quadrupled at the beginning of a 150-yr run). Additionally, for 11 available models (those denoted by asterisks in Table 1), we analyze the 30-yr-long sstClim and sstClim4×CO₂ scenarios, in which sea surface temperatures (SSTs) and sea ice concentrations are held fixed to the preindustrial control climatology for both preindustrial atmospheric CO₂ concentrations (sstClim) and quadrupled atmospheric CO₂ concentrations (sstClim4×CO₂). For all scenarios, we use the first ensemble member (“r1i1p1”) from each model.

To compare the model output with observations, we make use of three observational data sets: 1) monthly-mean top-of-the-atmosphere radiative fluxes from the Clouds and Earth’s Radiant Energy System (CERES) experiment (Energy Balanced and Filled top-of-atmosphere fluxes version 2.7; Loeb et al. 2012) obtained from the National Aeronautics and Space Administration (NASA) Langley Research Center; 2) monthly-mean visible–infrared satellite-detected cloud fractions from the International Satellite Cloud Climatology Project (ISCCP; Rossow and Schiffer 1999) obtained from the NASA Goddard Institute for Space Studies, and 3) monthly-mean zonal wind data from the European Centre for Medium-Range Weather Forecasts (ECMWF) Interim Re-Analysis (ERA-Interim; Dee et al. 2011). The CERES data cover the period March 2000–June 2013, and the ISCCP data cover the period July 1983–December 2009. The ERA-Interim data begin in 1979 and extend to the present. For the ISCCP data, we use two derived data products: 1) the top-of-the-atmosphere radiative fluxes (ISCCP-FD; Zhang et al. 2004) and 2) the simulator-oriented ISCCP cloud product produced for the Cloud Feedback Model Intercomparison Project (CFMIP;

TABLE 1. Listing of the CMIP5 models used in this study. Models with output from the sstClim and sstClim4×CO₂ scenarios are denoted with asterisks.

Model number	Model name	Modeling center
Type I models		
1*	BCC_CSM1.1 [Beijing Climate Center (BCC), Climate System Model, version 1.1]	BCC, China Meteorological Administration
2	BCC_CSM1.1-m (BCC, Climate System Model, version 1.1, moderate resolution)	BCC, China Meteorological Administration
3*	CanESM2 (Second Generation Canadian Earth System Model)	Canadian Centre for Climate Modelling and Analysis
4*	CCSM4 (Community Climate System Model, version 4)	National Center for Atmospheric Research
5	CNRM-CM5 [Centre National de Recherches Météorologiques (CNRM) Coupled Global Climate Model, version 5]	CNRM/Centre Européen de Recherche et Formation Avancés en Calcul Scientifique
6*	IPSL-CM5A-LR [L'Institut Pierre-Simon Laplace (IPSL) Coupled Model, version 5A, low resolution]	IPSL
7	MIROC-ESM (Model for Interdisciplinary Research on Climate, Earth System Model)	Japan Agency for Marine-Earth Science and Technology, Atmosphere and Ocean Research Institute (The University of Tokyo), and National Institute for Environmental Studies
8*	MPI-ESM-LR (Max Planck Institute Earth System Model, low resolution)	Max Planck Institute for Meteorology
9*	MPI-ESM-P (Max Planck Institute Earth System Model, paleo)	Max Planck Institute for Meteorology
10	NorESM1-M (Norwegian Earth System Model, version 1 (intermediate resolution))	Norwegian Climate Centre
Type II models		
11	ACCESS1.0 (Australian Community Climate and Earth-System Simulator, version 1.0)	Commonwealth Scientific and Industrial Research Organization (CSIRO), and Bureau of Meteorology, Australia
12*	CSIRO-Mk3.6.0 CSIRO Mark, version 3.6.0)	CSIRO in collaboration with the Queensland Climate Change Centre of Excellence
13*	GFDL CM3 [Geophysical Fluid Dynamics Laboratory (GFDL) Climate Model, version 3]	National Oceanic and Atmospheric Administration (NOAA)/GFDL
14	GFDL-ESM2G [GFDL Earth System Model with Generalized Ocean Layer Dynamics (GOLD) component]	NOAA/GFDL
15	GFDL-ESM2M [GFDL Earth System Model with Modular Ocean Model 4 (MOM4) component]	NOAA/GFDL
16	HadGEM2-ES (Hadley Centre Global Environment Model, version 2–Earth System)	Met Office Hadley Centre
17*	INM-CM4 (Institute of Numerical Mathematics Coupled Model, version 4.0)	Institute for Numerical Mathematics
18	IPSL-CM5B-LR (IPSL Coupled Model, version 5B, low resolution)	IPSL
19*	MIROC5 (Model for Interdisciplinary Research on Climate, version 5)	Atmosphere and Ocean Research Institute (The University of Tokyo), National Institute for Environmental Studies, and Japan Agency for Marine-Earth Science and Technology
20*	MRI-CGCM3 (Meteorological Research Institute Coupled Atmosphere–Ocean General Circulation Model, version 3)	Meteorological Research Institute

<http://climserv.ipsl.polytechnique.fr/cfmip-obs/>; Pincus et al. 2012; Zhang et al. 2012).

b. Methods

For each model, we construct a monthly time series of jet position by computing the latitude of the 850-hPa

zonal-mean, zonal wind maximum in the SH. The zonal wind maximum is found using a quadratic fit to the model data at a resolution of 0.01° (see appendix for further details). The 850-hPa level effectively captures the location of the midlatitude eddy-driven jet, while avoiding most topography and potential contamination from the

upper-tropospheric (angular momentum conserving) jet in the subtropics. Virtually identical jet variability can be identified using the leading principal component time series of the 850-hPa geopotential height field poleward of 20°S [i.e., the southern annular mode (SAM)]. However, because each model's SAM corresponds to a slightly different magnitude jet shift, we choose to perform our analysis using the jet latitude time series, such that regressions on this time series correspond to a 1° poleward jet shift for each model.

We quantify the impact of clouds on Earth's radiative budget through the cloud radiative effect (CRE) approach. CRE, which is also commonly referred to as cloud radiative forcing, is calculated as the difference in outgoing radiation at the top of the atmosphere between clear-sky and all-sky scenarios (e.g., Ramanathan et al. 1989; see also appendix). When examining the atmospheric response to greenhouse gas forcing, CRE calculations not only reflect changes in cloud radiative processes, but can also be contaminated by changes in temperature, water vapor, and surface albedo. For example, in a region with constant cloud cover, melting sea ice would decrease the clear-sky surface albedo, and hence artificially produce a negative shortwave CRE anomaly. In these situations, using a cloud radiative kernel approach is more accurate for isolating cloud radiative processes (Zelinka et al. 2012), but unfortunately only a small subset of CMIP5 models provides the necessary output for the kernel approach (see results in Zelinka et al. 2013). Consequently, in this study, we define the relationship between SH jet variability and cloud radiative processes using the preindustrial control scenario, where discrepancies between the CRE and kernel approaches are minimal.

3. Cloud radiative effects associated with SH jet variability in CMIP5 models

In this section, we quantify the CRE anomalies associated with a 1° poleward shift in the SH midlatitude jet in each of the CMIP5 models listed in Table 1. To do this, we use the preindustrial control run from each model (such that the jet variability is purely unforced) and regress the CRE anomalies (from the long-term mean) on the SH jet latitude time series (see appendix for further details). Here, we focus on the December–February (DJF) season, when the incoming solar radiation is maximized in the SH; virtually identical results (with weaker magnitude) are found in the annual mean.

Figure 1 shows the patterns of shortwave CRE anomalies associated with a 1° poleward jet shift in the preindustrial control climate of each of the 20 CMIP5 models. The patterns in Fig. 1 clearly demonstrate that the

shortwave CRE response to a poleward jet shift (which we refer to hereafter as shortwave jet–CRE) is not uniform across CMIP5 models. One can easily identify two classes of models visually. One class (type I models) exhibits large annular shortwave jet–CRE warming (as in G13), while the other class (type II models) exhibits weaker, less coherent jet–CRE patterns of varying sign and little zonally symmetric structure (as in K14).¹ Qualitatively similar patterns to those shown in Fig. 1 are found in the cloud albedo forcing (as defined by Tsushima et al. 2006) and total cloud fraction fields (not shown). Thus, the strong shortwave jet–CRE warming in type I models largely results from a reduction in total cloud fraction (and the associated reflection of sunlight) at SH midlatitudes as the jet moves poleward.

Figure 2 shows the corresponding patterns of longwave jet–CRE. In contrast to the shortwave jet–CRE patterns shown in Fig. 1, there is no noticeable distinction between the longwave jet–CRE patterns in the two classes of models. As in G13, the longwave jet–CRE is largely positive at high latitudes and in the subtropics, and negative at midlatitudes. Because longwave CRE primarily reflects the behavior of high clouds, the agreement among the models in Fig. 2 implies that low clouds are likely responsible for the differences in the shortwave jet–CRE patterns shown in Fig. 1. We will discuss this point further in section 4.

To summarize the results in Figs. 1 and 2, we show in Fig. 3 the composite jet–CRE patterns for type I and type II models. As noted above, the composite longwave jet–CRE patterns for the two classes of models are virtually identical (Fig. 3a). The key difference in the jet–CRE patterns between the two classes of models arises from the shortwave contribution at SH midlatitudes (30°–60°S) (Fig. 3b). This is most readily apparent in the zonal mean (Fig. 3c). The large shortwave jet–CRE maximum at SH midlatitudes in type I models contributes to a small hemispherically integrated warming effect (reported in the box in Fig. 3c, left), whereas the midlatitude jet–CRE features in type II models contribute to a small hemispherically integrated cooling effect (Fig. 3c, right). Because the SH midlatitude jet shifts poleward in response to many anthropogenic forcings (e.g., Kushner et al. 2001; Polvani et al. 2011), this result may have important implications for climate model predictions (see section 5).

¹ The model used in K14, the Community Earth System Model, version 1, coupled with the Community Atmosphere Model, version 5 (CESM-CAM5), exhibits the behavior of a type II model. We do not include this model in our study because it did not provide an abrupt 4×CO₂ integration for the CMIP5 archive.

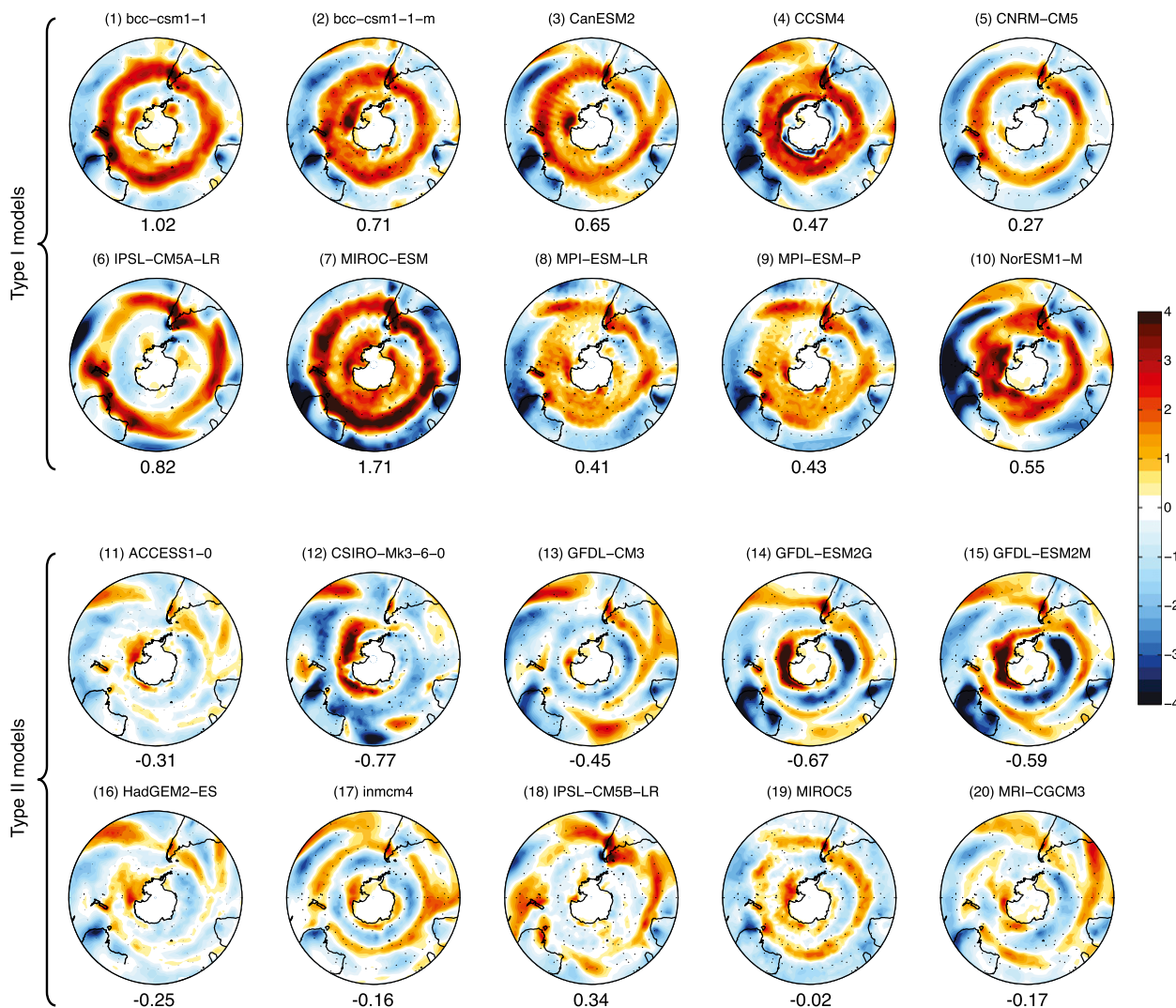


FIG. 1. Regressions of shortwave cloud radiative effect (CRE) anomalies (from the long-term mean) on the SH jet latitude time series from each of the indicated CMIP5 models (see Table 1). These shortwave jet-CRE patterns are calculated for the December-February (DJF) season, in the preindustrial control climate of each model. The contour interval is 0.25 W m^{-2} . Units correspond to a 1° poleward jet shift. The numbers below each panel display the values in that panel averaged over 30° - 60°S , which we refer to as the shortwave jet-CRE index.

One might question our categorization of type I and type II models in this section using visual analysis alone, but nearly identical results can be derived quantitatively. Averaging the shortwave jet-CRE over the 30° - 60°S latitude band clearly distinguishes the two classes of models (see also Fig. 3c), and these values (which we refer to hereafter as the shortwave “jet-CRE index”) are noted below each panel in Fig. 1. All the type I models have a positive (warming) value of the index, whereas all but one type II model have a negative (cooling) value of the index. The one outlier (model 18; see Table 1) visually appears to be a type II model, but quantitatively fits with the type I models. In the remaining figures, we will underline results from this particular model, which exhibits hybrid behavior.

4. Comparison with observations

In this section, we compare the jet-CRE patterns from CMIP5 models with those derived from recent observations, in order to determine which class of models has more realistic behavior. The jet-CRE patterns derived from the models’ historical runs are very similar to those derived from their preindustrial control runs (as shown in Figs. 1-3), and are not shown here for brevity.

Figure 4 shows the observed jet-CRE patterns derived using radiative fluxes from the ISCCP-FD and CERES datasets and zonal winds from the ERA-Interim reanalysis. The observed longwave jet-CRE patterns from both ISCCP-FD and CERES are very similar to those in

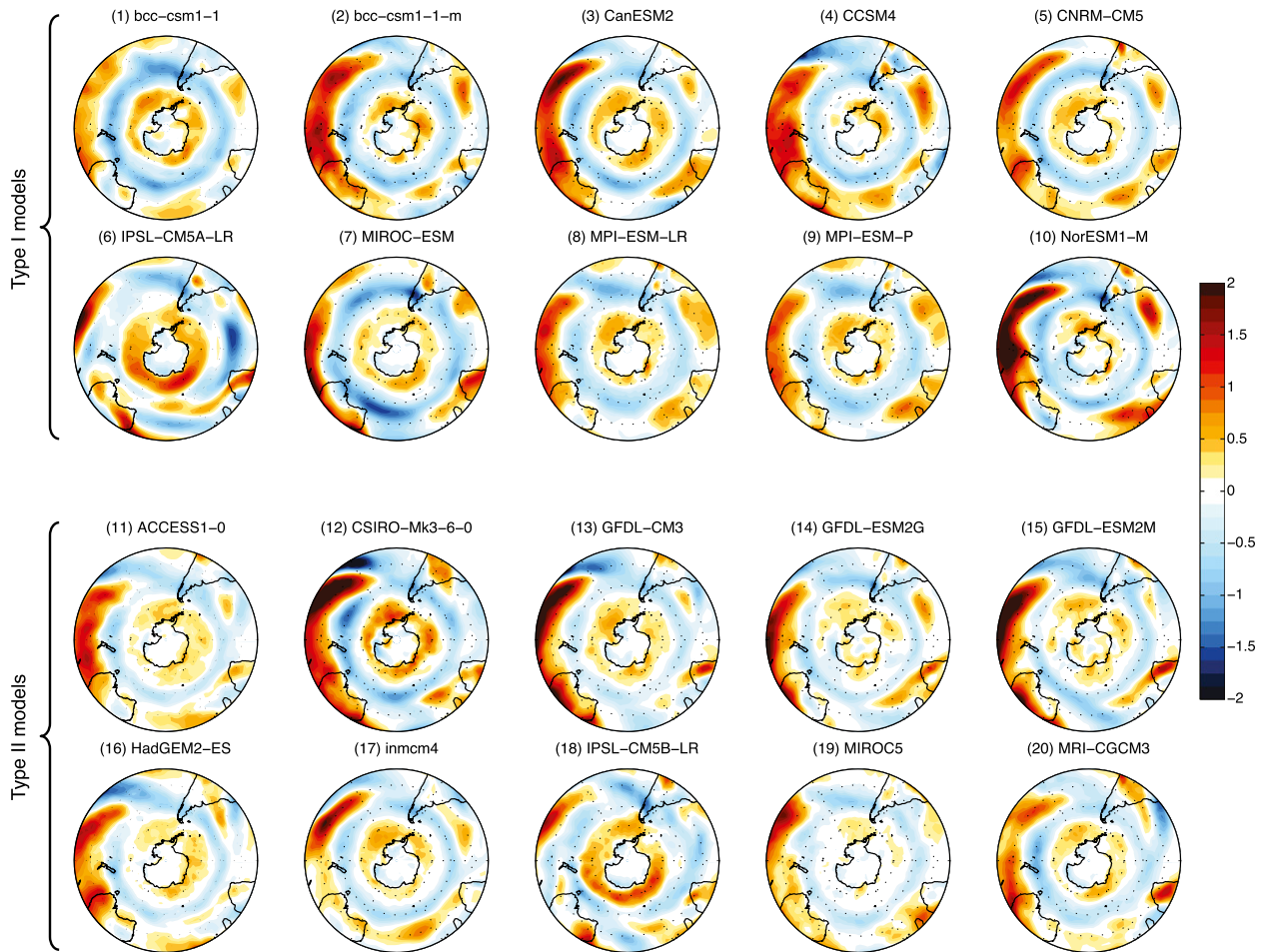


FIG. 2. As in Fig. 1, but for the longwave jet-CRE patterns. The contour interval is 0.125 W m^{-2} .

both classes of CMIP5 models (cf. Figs. 4a and 3a), suggesting that the longwave jet-CRE behavior in all of the models is quite realistic. In contrast, the observed shortwave jet-CRE patterns do not exhibit an annular warming at SH midlatitudes, as the type I models do (cf. Figs. 4b and 3b, left). Instead, the observed shortwave jet-CRE patterns at SH midlatitudes appear more regional in nature, with cooling over the Australian-Pacific sector and warming east of South America. Although noisy, these regional patterns qualitatively resemble those from many type II models (cf. Figs. 4b and 3b, right). We caution, however, that the observed patterns are based on limited periods of data and have only weak statistical significance. Nevertheless, as described below, we believe that it is not coincidental that the shortwave jet-CRE patterns in type II models resemble those from two independent observational datasets. Note also that the values of the shortwave jet-CRE index for the two observational datasets (-0.50 W m^{-2} for ISCCP-FD and -0.34 W m^{-2} for CERES) are comparable to those calculated for type II models (see Fig. 1).

In a previous paper (G13), we examined the cloud fraction anomalies associated with a poleward SH jet shift in a single type I model (CAM3) and found a relatively good correspondence with ISCCP observations (see Fig. 3 of G13). At first glance, these results seem to contradict those in Fig. 4. Interestingly enough, the high, middle, and low cloud fraction anomalies associated with a poleward SH jet shift (as examined in G13) are qualitatively very similar in observations, type I models, and type II models (not shown). However, cloud fraction anomalies can be potentially misleading, as they do not directly indicate the radiative properties of the clouds. Hence, it is only when the jet-CRE field is directly examined, as we do here, that the biases in type I models become more readily apparent (contrast Figs. 3b and 4b).

To explore the origin of the unrealistic shortwave jet-CRE patterns in type I models, we next examine the present-day DJF shortwave CRE climatologies from the CMIP5 models, and compare them to observations from CERES in Figs. 5 and 6. In the zonal mean (Fig. 5a), all

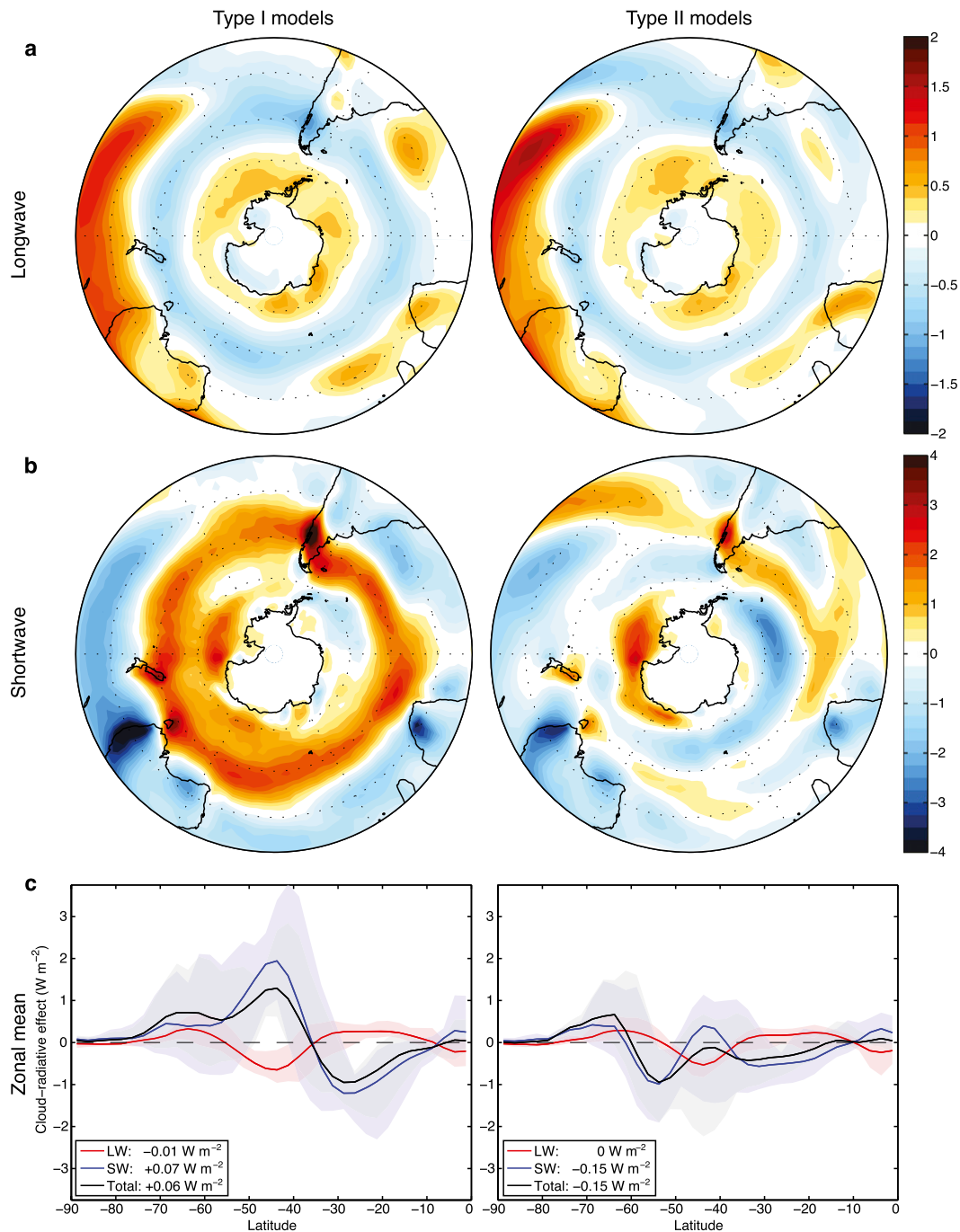


FIG. 3. (a),(b) Composites of the longwave and shortwave jet-CRE patterns shown in Figs. 1 and 2 for (left) type I models and (right) type II models. Corresponding (c) zonal average of the longwave (LW), shortwave (SW), and total jet-CRE patterns. The shaded error bounds denote the multimodel spread. Values averaged over the SH are listed in the legend.

models display a climatological minimum in shortwave CRE (i.e., a maximum in cloud reflection of incident solar radiation) over the Southern Ocean, but the values differ drastically among models (see also Ceppi et al. 2012). In fact, for the DJF season, the largest spread among the

models is not found in the tropics, but in the SH mid-latitudes. There, the type II models cluster around a minimum value of approximately -110 W m^{-2} , whereas the type I models cluster around a minimum value of approximately -140 W m^{-2} . The clustering of the models does

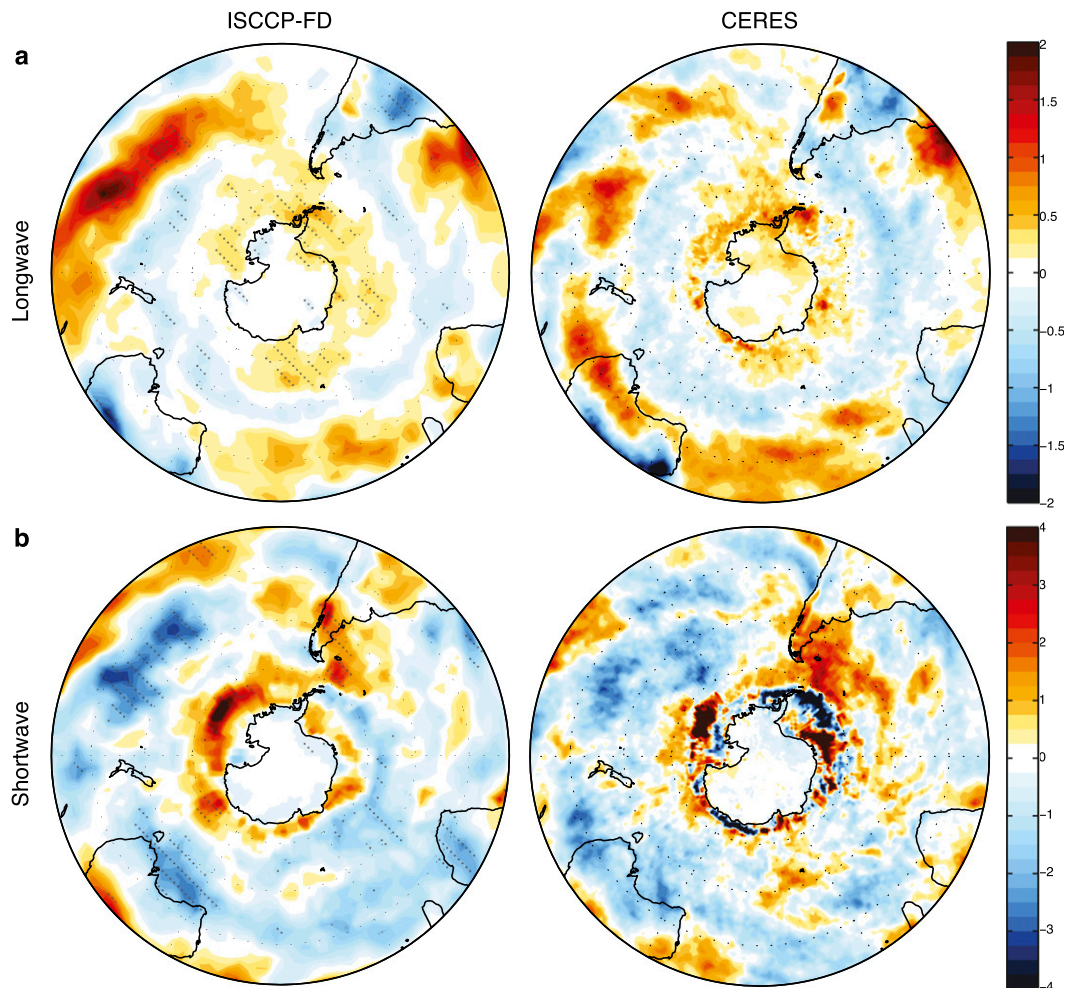


FIG. 4. As in Figs. 1 and 2, but for the observed jet-CRE patterns calculated using the monthly-mean DJF (left) ISCCP-FD (December 1983–December 2004) and (right) CERES (December 2000–February 2013) datasets, and the time series of the jet latitude derived from the ERA-Interim reanalysis. The stippling indicates regions that are 95% significant using Student's *t* test.

not appear to be by chance. As shown in Fig. 5b, for these models, the shortwave jet-CRE index is significantly correlated ($r = -0.75$) with the climatological minimum in shortwave CRE at SH midlatitudes.² Thus, models with greater climatological reflection of incident shortwave radiation by Southern Ocean clouds also generally have more positive shortwave jet-CRE values at SH midlatitudes.

An apparent paradox arises from the results in Figs. 4 and 5: The zonal-mean shortwave CRE climatology of type I models appears to be a better match for the CERES observations (cf. green and red lines in Fig. 5a),

even though these same models were shown to have unrealistically positive shortwave jet-CRE values at SH midlatitudes (cf. Figs. 3b and 4b). To help resolve this paradox, Fig. 6 shows maps of the present-day DJF shortwave CRE climatologies from CERES and the two classes of CMIP5 models. In type I models, the magnitude of the shortwave CRE over the Southern Ocean appears similar to observations (see also Fig. 5a), but the structure of the cloud reflection appears much too widespread and zonally symmetric (cf. Figs. 6a and 6b). In type II models, the magnitude of the shortwave CRE over the Southern Ocean is underestimated, but the spatial structure of the cloud reflection is less zonally symmetric and compares better with observations (cf. Figs. 6a and 6c). For example, both the CERES observations (Fig. 6a) and type II models (Fig. 6c) possess

²The climatological minima in shortwave CRE are nearly identical in the historical (Fig. 5a) and preindustrial control (Fig. 5b) climates of each CMIP5 model.

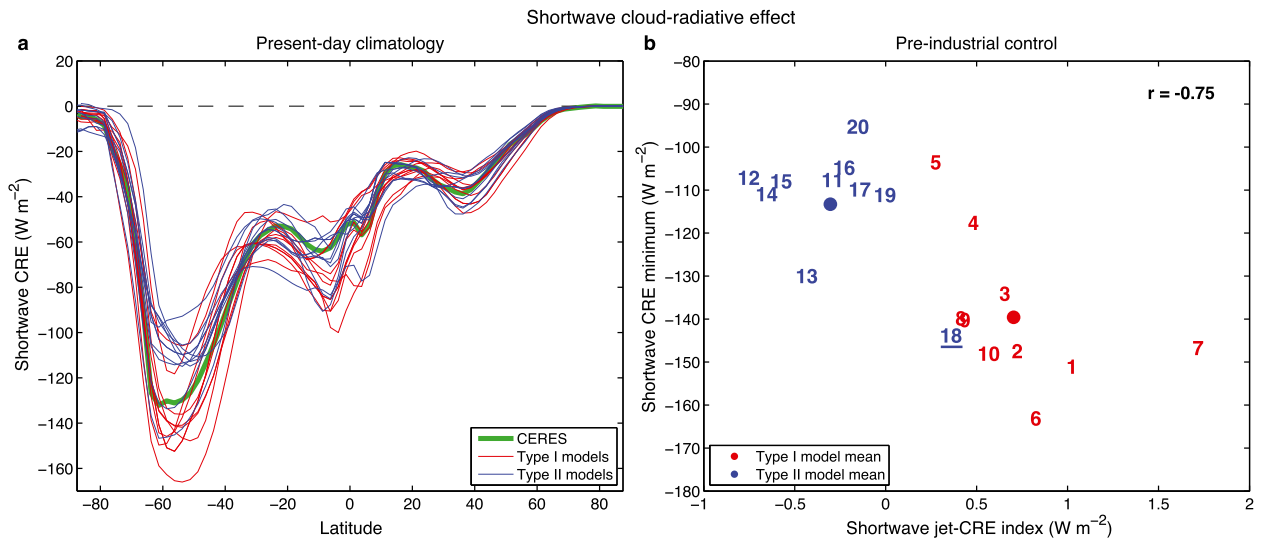


FIG. 5. (a) Present-day DJF zonal-mean shortwave CRE climatology for CERES observations (green) and individual type I (red) and type II (blue) CMIP5 models. The CERES climatology is derived from the 13 yr of available satellite observations (December 2000–February 2013), and the model climatologies are derived from the last 13 yr of the CMIP5 historical scenario (1993–2005). (b) Scatterplot between (abscissa) the shortwave jet–CRE index for each CMIP5 model and (ordinate) the climatological minimum in shortwave CRE over the Southern Ocean for each model [as shown in (a) for the present-day climatology]. Numbers on the scatterplot correspond to the models identified in Fig. 1. Calculations in (b) are for the DJF season, in the preindustrial control climate of each model.

distinct climatological minima in the southern Atlantic and Indian Oceans (45° – 60° S, 60° W– 60° E) and in the southwestern Pacific Ocean (50° – 65° S, 180° – 120° W). Interestingly, the composite of type II models is also closer to observations in the SH subtropical ocean basins, where the model representation of stratocumulus and cumulus-to-stratocumulus transition regimes has traditionally been problematic (e.g., Williams and Webb 2009; Klein et al. 2013).

To support our conclusion that the cloud structures in type II models are more realistic, we present the climatological optical depth distribution of Southern Ocean (40° – 60° S) clouds from ISCCP observations and the two classes of CMIP5 models (Fig. 7). The results in this figure are based upon a limited number of models, as the ISCCP simulator output necessary to produce this figure is only available from two type I models and three type II models (see Zelinka et al. 2013). The optical depth distributions of high-level and midlevel clouds appear to be similar in the available type I and II models (Figs. 7a,b), although both classes of models underestimate the observed amount of midlevel clouds. The differences between type I and II models appear to arise from an overabundance of optically thick, low-level clouds in type I models (Fig. 7c). This is a longstanding problem among climate models, which has been somewhat mitigated in many of the newest model versions (Kay et al. 2012; Klein et al. 2013).

To summarize: the key result of our analysis is that type II models have a more realistic representation of

observed jet–CRE patterns over the Southern Ocean (cf. Figs. 3 and 4). The more realistic jet–CRE patterns in type II models appear to result from the models' ability to capture the observed spatial (Fig. 6) and optical depth (Fig. 7) distributions of low clouds over the Southern Ocean. Other factors might also contribute to the improved jet–CRE behavior in type II models. Because type I models have a more pronounced climatological minimum in shortwave CRE over the Southern Ocean (Fig. 5), one might expect them to also have a more equatorward-biased climatological jet latitude in the SH, as suggested by Ceppi et al. (2012). However, we find no significant difference in the jet latitudes between the two classes of models used here (as quantified in Table 2, fourth and fifth columns). This is not entirely surprising: the correlation between the Southern Ocean shortwave CRE climatology and the SH climatological jet latitude reported by Ceppi et al. (2012) is relatively weak, as it relies almost exclusively on the behavior of only a few outlying CMIP5 models (see Fig. 2 of Ceppi et al. 2012).

Based upon the results of this section, it would be tempting to naively argue that type II models have “better” clouds than type I models. While type II models accurately represent cloud processes directly tied to SH jet variability, they also misrepresent other key cloud processes, leading to an underestimate of the observed magnitude of shortwave CRE over the Southern Ocean (Fig. 5a)—and thus likely to an improper SH energy budget (see Trenberth and Fasullo 2010). Consequently,

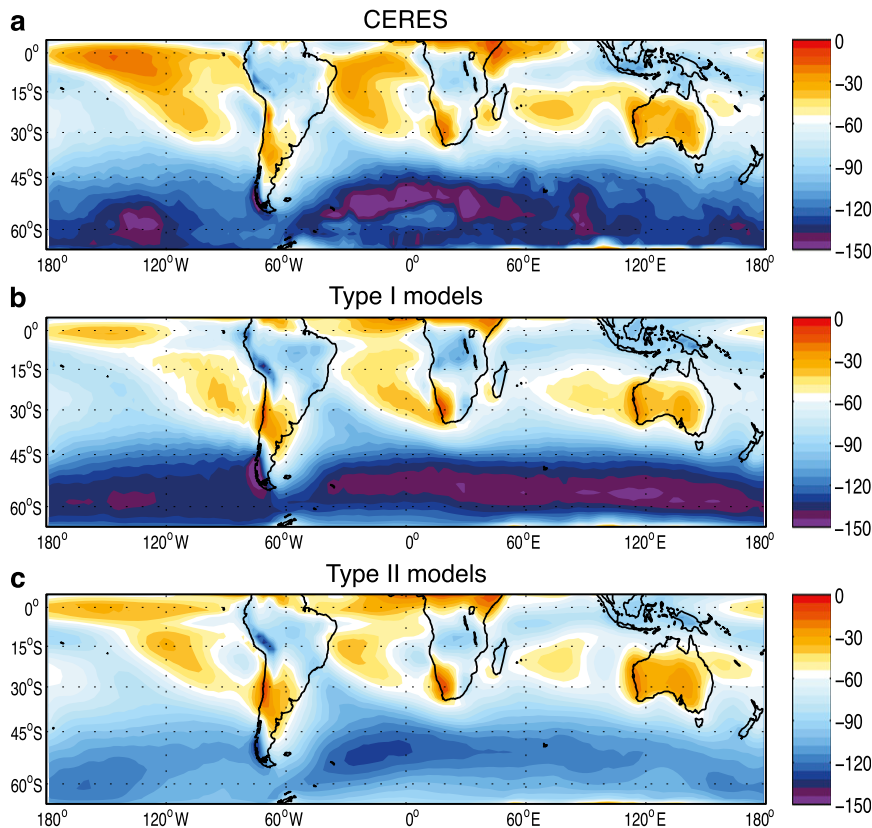


FIG. 6. Present-day DJF shortwave CRE climatology for (a) CERES observations, (b) type I models, and (c) type II models. The CERES climatology is derived from the 13 yr of available satellite observations (December 2000–February 2013), and the model climatologies are derived from the last 13 yr of the CMIP5 historical scenario (1993–2005). The model climatologies are a composite over all type I in (b) and type II in (c) models. The contour interval is 6 W m^{-2} .

both type I and type II models have strengths and weaknesses in their representation of observed cloud processes, and it is challenging to interpret why a trade-off exists between the models' representation of jet–CRE processes and their climatological magnitude of shortwave CRE. Further analyses of these model biases are left to a future study. For the remainder of this paper, we focus on the implications of the varying jet–CRE behavior in CMIP5 models.

5. Implications for climate projections

In this section, we discuss how the jet–CRE behavior in CMIP5 models may have important implications for the models' climate projections. It is well known that the SH midlatitude jet shifts robustly poleward in climate models in response to both stratospheric ozone depletion (Gillett and Thompson 2003; Son et al. 2008; Polvani et al. 2011) and enhanced greenhouse gas forcing (Kushner et al. 2001; Yin 2005; Barnes and Polvani 2013). Since the jet–CRE patterns in type I models contribute to a hemispherically

integrated warming effect (see Fig. 3c), one might expect the global warming in those models to exceed the warming in type II models when greenhouse gases are increased. To test this hypothesis, we examine the abrupt $4\times\text{CO}_2$ integrations from the CMIP5 archive. We focus on these integrations because they provide a large, simple, important, and unambiguous forcing of the climate system, and thus provide a much cleaner testbed for our hypothesis than the historical or representative concentration pathway (RCP) integrations. Recall that, in the historical and RCP integrations, many different forcings are applied, not all of which are identical across all models or are monotonically increasing over time (e.g., aerosols are increased then decreased in several scenarios).

Figure 8a shows the time series of the global-mean surface temperature response to the abrupt $4\times\text{CO}_2$ forcing in both classes of models. Note that the temperature response is plotted using a logarithmic time scale to emphasize the early years of the integrations. During the first 20 years of the runs, the type I models are indeed warming faster than the type II models (as

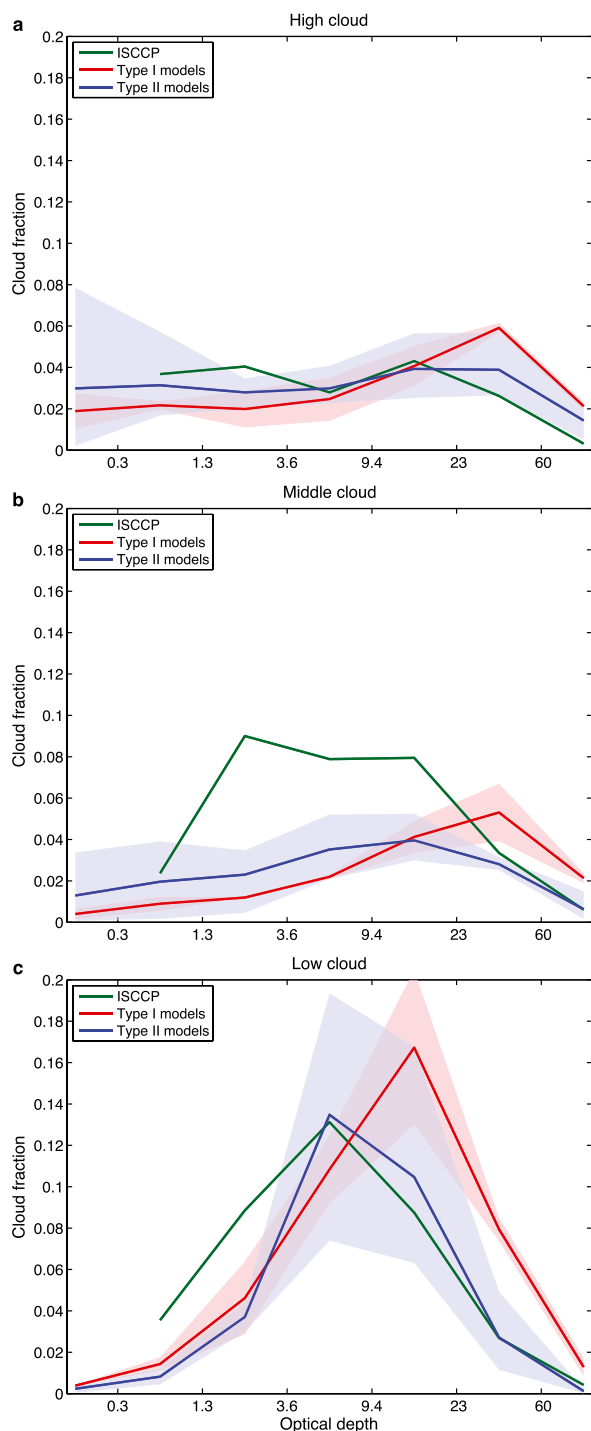


FIG. 7. The 1983–2005 DJF climatological distribution of cloud optical depth over the Southern Ocean (40° – 60° S): (a) high cloud fraction (cloud top pressure < 440 hPa), (b) middle cloud fraction (440 hPa < cloud top pressure < 680 hPa), and (c) low cloud fraction (cloud top pressure > 680 hPa). The observed climatology (green) is derived from the simulator-oriented ISCCP cloud product. Model climatologies are derived from the historical scenario of models that have ISCCP simulator output available: two type I models (CanESM2 and MPI-ESM-LR; red) and three type II models (HadGEM2-ES, MIROC5, and MRI-CGCM3; blue). Shading denotes the multimodel spread.

quantified in Fig. 8b).³ It is important to appreciate that the larger initial warming in the type I models is unlikely to occur by chance: randomly grouping the models into two subsets of 10 yields the separation seen in Fig. 8b only $\sim 1\%$ of the time (based on Monte Carlo tests of 1000 random model groupings).

Because type I models have a better representation of the observed climatological magnitude of shortwave CRE in the SH (Fig. 5), one might expect them to be warming more because, based on the CMIP3 findings of Trenberth and Fasullo (2010), they might have larger values of equilibrium climate sensitivity. However, after the initial period of larger warming in type I models, the global-mean surface temperature time series from the two classes of models begin to converge (albeit very slowly) (Fig. 8a), such that there is no significant difference between the equilibrium climate sensitivities of type I and II models (Fig. 8c; see also Table 2, third column).⁴ Instead, any significant difference in warming between type I and II models occurs in the very rapid, transient response of the models to increased greenhouse gas forcing. This is in agreement with other studies, which have identified cloud-induced shortwave warming as being largely responsible for the rapid (nonequilibrium) adjustment of the climate system to increased CO_2 levels (Andrews and Forster 2008; Colman and McAvaney 2011; Andrews et al. 2012a; Zelinka et al. 2013).

One might argue that the difference in the transient warming between the two classes of models (Fig. 8a) might have little to do with the jet–CRE biases, and be due to other differences among the models. To show that the SH jet–CRE biases are indeed key to the difference in warming between the two classes of models, in Fig. 9 we show maps of the difference in the surface temperature and shortwave CRE responses between the type I and type II models. For the first 20 years of the abrupt $4\times\text{CO}_2$ scenario, the bulk of the enhanced warming in the type I models arises from three regions in the SH (Fig. 9a). First, in the SH subtropics, the type I models have anomalous warming in regions where they poorly represent the observed shortwave CRE climatology (see Fig. 6). Second, at SH midlatitudes, the type I models have excess warming in regions where the shortwave jet–CRE biases occur (Fig. 1). And finally, at SH high latitudes,

³ The results in Fig. 8b are not sensitive to the choice of the first 20 years. Similar results are found using the first 5, 10, and 30 yr.

⁴ Calculations of equilibrium climate sensitivity are based on a linear regression fit [see plots in Gregory et al. (2004) and Andrews et al. (2012b)]. Thus, the disparity among type I and II models at the end of the abrupt $4\times\text{CO}_2$ scenario (year 150) in Fig. 8a is not necessarily comparable to the spread in the equilibrium climate sensitivities of the models.

TABLE 2. Characteristics of the indicated CMIP5 models. The equilibrium climate sensitivity (ECS) values in the third column are reproduced from Table 1 of Forster et al. (2013). The midlatitude jet characteristics in the fourth through seventh columns are calculated for the 850-hPa SH midlatitude jet [Negative values in the fourth and fifth columns denote degrees latitude for SH and in the sixth and seventh columns denote a southerly (poleward) shift in degrees latitude].

Model number	Model name	ECS (K)	DJF-mean jet lat (°) (control)	Annual-mean jet lat (°) (control)	DJF-mean jet shift (°) (4×CO ₂) (years 1–20)	Annual-mean jet shift (°) (4×CO ₂) (years 1–20)
Type I models						
1	BCC_CSM1.1	2.82	−46.77	−47.93	−2.48	−1.86
2	BCC_CSM1.1-m	2.87	−48.82	−49.73	−2.78	−2.36
3	CanESM2	3.69	−47.30	−48.05	−3.78	−2.71
4	CCSM4	2.89	−50.90	−51.75	−1.02	−1.45
5	CNRM-CM5	3.25	−47.00	−48.50	−2.07	−1.76
6	IPSL-CM5A-LR	4.13	−41.75	−41.94	−4.45	−4.70
7	MIROC-ESM	4.67	−43.75	−44.04	−1.90	−2.70
8	MPI-ESM-LR	3.63	−47.41	−47.34	−3.04	−3.25
9	MPI-ESM-P	3.45	−47.39	−47.35	−2.47	−2.97
10	NorESM1-M	2.80	−49.34	−50.95	−1.96	−2.01
	Mean ± 1σ	3.42 ± 0.63	−47.04 ± 2.64	−47.76 ± 2.96	−2.59 ± 0.98	−2.58 ± 0.94
Type II models						
11	ACCESS1.0	3.83	−48.17	−50.27	−2.68	−1.62
12	CSIRO-Mk3.6.0	4.08	−48.34	−47.36	−2.49	−2.02
13	GFDL CM3	3.97	−47.57	−48.45	−2.85	−2.77
14	GFDL-ESM2G	2.39	−48.55	−49.75	−2.57	−2.10
15	GFDL-ESM2M	2.44	−47.78	−49.05	−2.17	−1.99
16	HadGEM2-ES	4.59	−49.00	−50.16	−3.24	−1.91
17	INM-CM4	2.08	−49.44	−49.19	−1.87	−1.67
18	IPSL-CM5B-LR	2.61	−42.95	−43.40	−1.05	−1.54
19	MIROC5	2.72	−47.55	−46.78	−2.28	−3.46
20	MRI-CGCM3	2.60	−47.80	−50.18	−1.58	−0.74
	Mean ± 1σ	3.13 ± 0.89	−47.71 ± 1.79	−48.46 ± 2.14	−2.28 ± 0.64	−1.98 ± 0.73

the type I models are warming more near the Antarctic coastline.

The enhanced warming in type I models primarily occurs in regions where their shortwave CRE response to the abrupt 4×CO₂ forcing is significantly more positive (Fig. 9b). In the SH subtropics and midlatitudes, similar discrepancies between the shortwave CRE responses of type I and II models also occur in analogous experiments with fixed SSTs (Fig. 9c). Hence, in these regions, rapid cloud adjustments due to CO₂ forcing alone (in the absence of SST changes) contribute to enhanced warming in type I models. However, near the Antarctic coastline, the shortwave CRE response is biased negative in regions where cloud cover is positioned above melting sea ice (Fig. 9b; see also section 2b). In this region, sea ice and SST changes appear central to the enhanced warming in type I models, as differences in the shortwave CRE responses between the two classes of models largely vanish when SSTs and sea ice concentrations are held fixed (Fig. 9c).

With the differences in the SH subtropics and high latitudes duly noted, we now focus on the SH midlatitudes, where the jet–CRE biases appear to play a key role in the

surface temperature response to CO₂ forcing (Fig. 9). To confirm the role of the jet–CRE biases, we plot, in the left column of Fig. 10, time series of the response of the SH midlatitude jet, shortwave CRE, and surface temperature to the abrupt 4×CO₂ forcing, for both type I and type II models. In both types of models, the jet shifts rapidly poleward in the first few years after the CO₂ forcing is imposed, and largely reaches its equilibrium position within a couple of decades, as seen in Fig. 10a.

Ceppi et al. (2014) have recently suggested that a strong relationship exists in the CMIP5 models between the magnitude of the poleward jet shift and the shortwave CRE response to climate change (via SST changes), but our results appear inconsistent with their findings. While the multimodel mean jet shift for the type I models is consistently more poleward than that of the type II models (cf. red and blue lines in Fig. 10a), we find that the difference in the poleward jet shifts between the two subsets of models considered here is not statistically significant. The difference in the poleward jet shifts between the two classes of models is neither significant at the beginning of the abrupt 4×CO₂ integrations (i.e., the first 20 yr, as quantified in the sixth

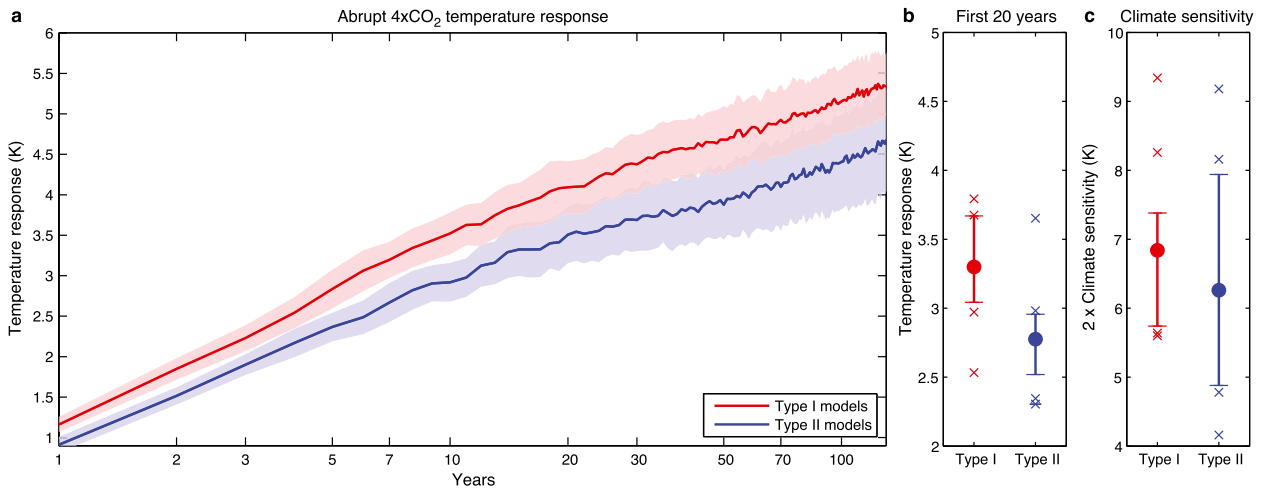


FIG. 8. Global-mean surface temperature response to abrupt quadrupling of CO_2 in CMIP5 models. (a) Composite annual-mean time series for type I (red) and type II (blue) models. Results are derived as the difference between the abrupt $4\times\text{CO}_2$ scenario for each model and its preindustrial control climatology. Shading denotes 90% confidence intervals. (b) Scatter of individual model responses averaged over the first 20 yr of the abrupt $4\times\text{CO}_2$ scenario. For each type of model, the circle denotes the multimodel mean, the bar denotes the range of the 25th–75th percentiles, and each diagonal cross denotes outliers about the 25th–75th percentiles. (c) As in (b), but for twice the individual model values of equilibrium climate sensitivity (from Forster et al. 2013). The equilibrium climate sensitivity values are doubled, so that all panels in the figure correspond to a $4\times\text{CO}_2$ climate.

and seventh columns of Table 2) nor significant at the end of the abrupt $4\times\text{CO}_2$ integrations (i.e., the last 50 yr; not shown).

To clarify the role of SSTs in the jet shifts, in the right column of Fig. 10a, we show the responses of the SH midlatitude jet to $4\times\text{CO}_2$ forcing (as in Fig. 10a, left), but with SSTs held fixed. The results reveal that CO_2 forcing alone (in the absence of SST changes) can induce a modest jet shift (see also Staten et al. 2012), demonstrating that SST-mediated feedbacks cannot be the sole cause of the jet shifts. Although global-mean surface temperatures remain largely unchanged with the abrupt quadrupling of atmospheric CO_2 concentrations (Fig. 10c, right), the SH midlatitude jet shifts poleward in all but one of the available models.

Interestingly, in the fixed SST runs, we find a significant difference between the jet shifts in the two classes of models. However, if differences in the models' shortwave CRE responses were partially forcing the jet shifts through SST changes [as Ceppi et al. (2014) argue], one might expect a more significant difference between the jet shifts of type I and type II models in the fully coupled runs (Fig. 10a, left; Table 2, sixth and seventh columns), rather than in the fixed SST runs (Fig. 10a, right). This is not the case here, and therefore we find no evidence in our results to support the mechanism proposed by Ceppi et al. (2014).

Unlike the small differences in jet shifts between type I and type II models, we find a large, significant difference between the responses of the models' shortwave CRE at

SH midlatitudes ($35^\circ\text{--}50^\circ\text{S}$, see boxed region in Fig. 9b), in both the fully coupled (Fig. 10b, left) and fixed SST (Fig. 10b, right) experiments. As one can see in Fig. 10b (left), an initial shortwave CRE response of $\sim 3.5 \text{ W m}^{-2}$ occurs within the first two years after CO_2 quadrupling in type I models, whereas the initial shortwave CRE response is approximately zero in type II models. This confirms our hypothesis: while the jet shifts rapidly poleward in both types of models, only those models that produce a shortwave cloud radiative warming effect in association with unforced poleward jet shifts (i.e., type I models) also produce a rapid shortwave cloud radiative warming effect in response to CO_2 forcing. In fact, the magnitude of the initial (first 5 yr) shortwave CRE response in each model (Fig. 10b, left) is significantly correlated ($r = 0.90$) with its shortwave jet–CRE index derived from preindustrial control variability, as seen in the scatterplot in Fig. 11. Consequently, the same processes that are relevant for the interannual jet–CRE variability in the models are also relevant for the nearly instantaneous, transient response of the models to CO_2 forcing. Again, note that this occurs irrespective of whether the SSTs are fixed or not.

Finally, we address the issue of time scales. Although the initial response of the models' shortwave CRE is strongly linked to the jet–CRE biases, it is interesting to note that the time series of the SH midlatitude shortwave CRE response in Fig. 10b (left) also show a slow increase over the duration of the abrupt $4\times\text{CO}_2$ scenario for both type I and type II models. That slowly increasing

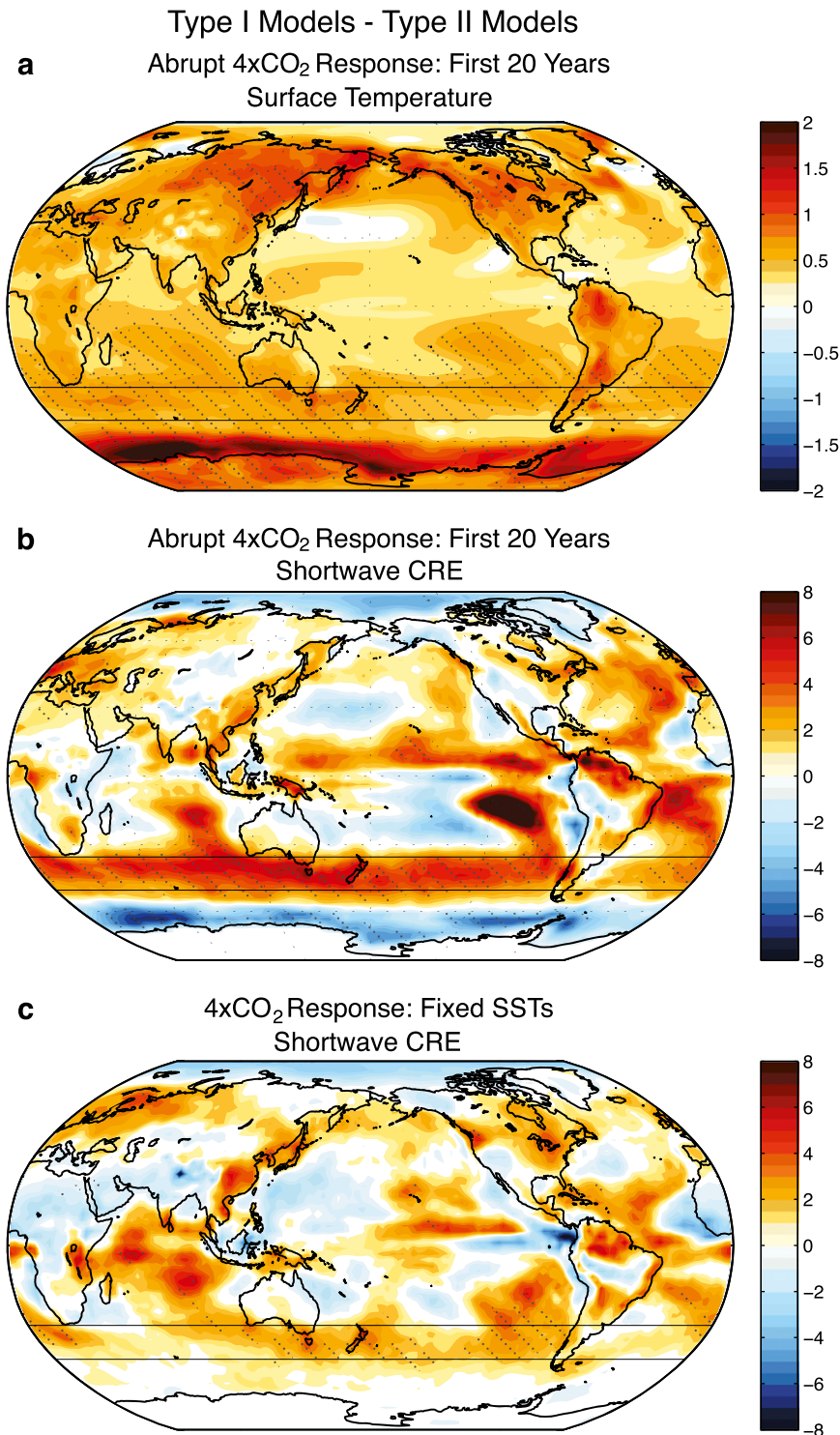


FIG. 9. Differences in the composite annual-mean responses to $4\times\text{CO}_2$ forcing between type I and type II models (i.e., type I response – type II response). For each model, the responses are derived as the difference between (a),(b) the abrupt $4\times\text{CO}_2$ scenario (averaged over the first 20 yr) and the corresponding preindustrial control climatology and (c) the $4\times\text{CO}_2$ and control scenarios with fixed sea surface temperatures (sstClim $4\times\text{CO}_2$ and sstClim), which are available only from 11 models (see Table 1). The contour interval is 0.125 K in (a) and 0.5 W m^{-2} in (b),(c). Stippling indicates regions where the model composites are different at the 95% statistically significant level. The horizontal lines denote the $35^\circ\text{--}50^\circ\text{S}$ latitude band.

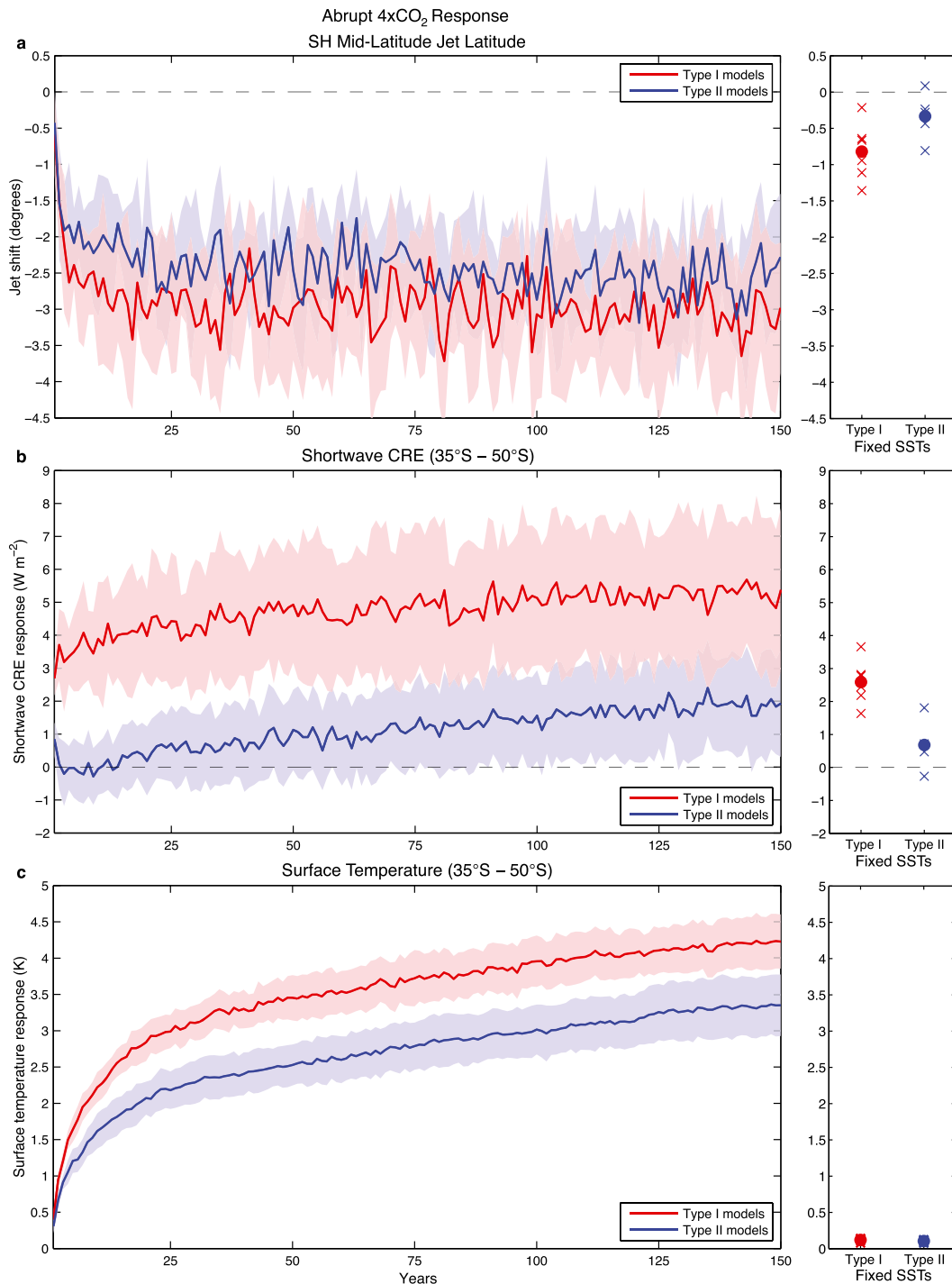


FIG. 10. Response to abrupt quadrupling of CO₂ in CMIP5 models. (a) On the left is the composite annual-mean time series of the SH midlatitude jet latitude for (red) type I models and (blue) type II models. Results are derived as the difference between the abrupt 4×CO₂ scenario for each model and its preindustrial control climatology. Shading denotes 90% confidence intervals. On the right is the scatter of SH midlatitude jet latitude responses to 4×CO₂ forcing with fixed SSTs (i.e., the difference between the climatologies of the sstClim4×CO₂ and sstClim scenarios). For each type of model, the circle denotes the multimodel mean. (b) As in (a), but for the shortwave CRE averaged over 35°–50°S. (c) As in (a), but for the surface temperature averaged over 35°–50°S.

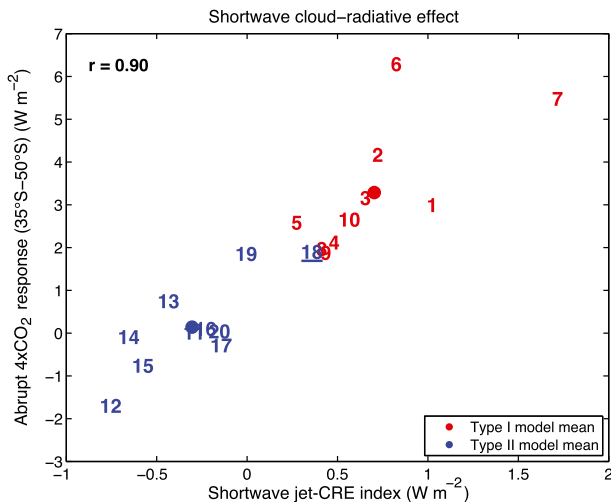


FIG. 11. As in Fig. 5b, but for the scatterplot between (abscissa) the shortwave jet-CRE index for each CMIP5 model and (ordinate) the initial (first 5 yr) response of shortwave CRE ($35^{\circ}\text{--}50^{\circ}\text{S}$) to abrupt $4\times\text{CO}_2$ forcing. The response is derived as the difference between the abrupt $4\times\text{CO}_2$ scenario for each model and its preindustrial control climatology (see Fig. 10b). A virtually identical scatterplot can be produced using the response of shortwave CRE averaged over the $30^{\circ}\text{--}60^{\circ}\text{S}$ latitude band on the ordinate ($r = 0.85$).

shortwave CRE response does not closely follow the midlatitude jet response (Fig. 10a, left), but instead that of the steadily increasing global-mean surface temperature (Fig. 8a). Thus, as argued by K14, thermodynamic influences are also a key factor in explaining the shortwave CRE response at SH midlatitudes, particularly as the equilibrium climate is approached.

In summary, we have found a direct link between the model jet-CRE biases and the rapid response of the models to abrupt $4\times\text{CO}_2$ forcing. In response to CO_2 forcing, the SH midlatitude jet shifts rapidly poleward in all models (Fig. 10a), but only the type I models exhibit a rapid shortwave CRE response at SH midlatitudes (Figs. 9b, 10b, and 11). And while the initial shortwave CRE response is very rapid, it has a direct impact on the surface temperatures at SH midlatitudes that lasts over a century (Figs. 9a and 10c), and is a key contributor to the difference in global-mean surface temperature warming between the two types of models (Fig. 8a). Note that the widely used equilibrium climate sensitivity, which is concerned with asymptotic stages of the response to CO_2 quadrupling, masks the jet-CRE biases, which manifest themselves at the very early stages of the response.

6. Summary and conclusions

In this study, we examined the linkages between variability in the SH midlatitude jet and cloud radiative

processes in CMIP5 models. Previous studies have often concluded that, as the jet moves poleward, the bulk of the clouds will move poleward with the jet, contributing to increased solar warming at SH midlatitudes (e.g., Bender et al. 2012; G13). We find that this behavior indeed exists in roughly half of the CMIP5 models (type I models) examined here. However, other CMIP5 models do not exhibit this behavior. Instead, as for the model examined by K14, the shortwave jet-CRE patterns in this second class of models (type II models) are weaker and less zonally symmetric in structure (Fig. 3b). Contrary to our expectations, it is this second class of models that compares better with observed jet-CRE patterns (Fig. 4), even though these same models substantially underestimate the observed climatological magnitude of shortwave cloud reflection at SH midlatitudes (Fig. 5a). The more realistic jet-CRE patterns in type II models appear to arise from the models' ability to capture the zonally asymmetric cloud structures observed over the Southern Ocean (Fig. 6), and to more accurately simulate the optical depth of low clouds in this region (Fig. 7).

The jet-CRE biases in the CMIP5 models are not simply a peculiar feature of the models' internal variability: these biases have direct relevance for most climate change scenarios, in which the position of the SH midlatitude jet shifts poleward with increased greenhouse gases. We find that the nearly instantaneous response of the global-mean surface temperature to abrupt CO_2 forcing is significantly larger in type I models (Fig. 8), and this excess warming arises largely from regions of reduced shortwave cloud reflection in the SH subtropics and midlatitudes (Fig. 9). We find strong evidence that the same processes that contribute to the jet-CRE biases in type I models also contribute to their larger initial warming response to CO_2 forcing (Figs. 10 and 11).

Since type II models have a more realistic representation of the observed jet-CRE patterns, it is reasonable to argue that they might also be more accurate in representing the response to CO_2 forcing. As a consequence, because at least half of the CMIP5 models are of type I, the transient global-mean surface temperature warming might be overestimated in the CMIP5 multimodel mean. Indeed, others have recently noted that the transient warming rates might be too high in some CMIP5 models (Stott et al. 2013; Otto et al. 2013; Fyfe et al. 2013). However, the type II models also have deficiencies, including the underestimate of the observed shortwave cloud reflection over the Southern Ocean (Fig. 5a), and an underestimate of Southern Ocean cloud cover has been linked to an underestimate of the equilibrium climate sensitivity and thus to an underestimate of the global warming response (cf. Fig. 13 of Trenberth and Fasullo 2010).

So, are type I models warming too much in response to CO₂ forcing (as the jet–CRE analysis in this study seems to imply)? Or are type II models warming too little [as could be hypothesized from the CMIP3 results of Trenberth and Fasullo (2010)]? At least for the CMIP5 models examined here, we find no evidence that the equilibrium climate sensitivity is significantly different between the two classes of models (Fig. 8c; Table 2, third column). Instead, we find that the significant difference between the two classes of models arises from the rapid response to abrupt CO₂ forcing, exactly when the type I models exhibit an additional shortwave cloud radiative warming effect at SH mid-latitudes that is strongly correlated with their jet–CRE biases (Figs. 10 and 11). However, as the models equilibrate to the CO₂ forcing, the warming in the two classes of models converges, so the equilibrium climate sensitivity remains similar (Fig. 8). Future work is thus needed to address to what degree the processes isolated here are of consequence in the more realistic, transient climate model simulations of the twentieth and twenty-first centuries.

Acknowledgments. We thank Y.-T. Hwang, M. D. Zelinka, and three anonymous reviewers for helpful comments on the manuscript. We also thank H. Liu for assistance in obtaining CMIP5 data, E. A. Barnes for providing us with the jet latitude code, and J. E. Kay and B. Medeiros for useful conversations during the preparation of this manuscript. We acknowledge the World Climate Research Programme’s Working Group on Coupled Modeling, which is responsible for CMIP, and we thank the climate modeling groups (listed in Table 1) for producing and making available their model output. For CMIP, the U.S. Department of Energy’s Program for Climate Model Diagnosis and Intercomparison provides coordinating support and led development of software infrastructure in partnership with the Global Organization for Earth System Science Portals. K.M.G. and L.M.P. are supported by a National Science Foundation grant to Columbia University.

APPENDIX

Method to Calculate Jet–CRE

In this appendix, we explicitly outline the methodology used to produce the jet–CRE patterns shown in Figs. 1 and 2, in order to ensure future reproducibility of our results.

We derive CRE (R_{CRE}) as the difference between the top-of-the-atmosphere outgoing clear-sky radiation R_{clear} (CMIP5 variables *rsuts* for shortwave and *rluts* for longwave) and the top-of-the-atmosphere outgoing radiation

R (CMIP5 variables *rsut* for shortwave and *rlut* for longwave):

$$R_{\text{CRE}} = R_{\text{clear}} - R. \quad (\text{A1})$$

The total CRE is defined as the sum of the shortwave CRE and longwave CRE.

As in Barnes and Polvani (2013), we derive the latitude of the SH midlatitude jet ϕ_{u850} as follows: 1) we find the grid point i with the maximum 850-hPa zonal-mean, zonal wind in the SH; 2) a quadratic is fit to the 850-hPa zonal-mean, zonal wind profile at grid points $i - 1$, i , and $i + 1$; and 3) ϕ_{u850} is defined as the latitude of the maximum of the quadratic fit (at a resolution of 0.01° latitude).

To find the jet–CRE patterns, we remove the time mean from the ϕ_{u850} time series to yield the ϕ'_{u850} time series, and we remove the time mean from the R_{CRE} time series at each latitude–longitude grid point (i, j) to yield the $R'_{\text{CRE}_{ij}}$ time series. (The time mean is removed as a function of month for monthly-mean data.) Then, the jet–CRE value at each latitude–longitude grid point ($R_{\text{jet-CRE}_{ij}}$) is defined as the linear regression coefficient between ϕ'_{u850} and $R'_{\text{CRE}_{ij}}$, where the overbar denotes the time mean, that is,

$$R_{\text{jet-CRE}_{ij}} = \frac{\overline{R'_{\text{CRE}_{ij}} \phi'_{\text{u850}}}}{\overline{\phi'^2_{\text{u850}}}}. \quad (\text{A2})$$

This is the quantity plotted in Figs. 1 and 2 for the shortwave and longwave, respectively. Finally, the jet–CRE index is defined as $R_{\text{jet-CRE}_{ij}}$ averaged over 30°–60°S.

REFERENCES

- Andrews, T., and P. M. Forster, 2008: CO₂ forcing induces semi-direct effects with consequences for climate feedback interpretations. *Geophys. Res. Lett.*, **35**, L04802, doi:10.1029/2007GL032273.
- , J. M. Gregory, P. M. Forster, and M. J. Webb, 2012a: Cloud adjustment and its role in CO₂ radiative forcing and climate sensitivity: A review. *Surv. Geophys.*, **33**, 619–635, doi:10.1007/s10712-011-9152-0.
- , —, M. J. Webb, and K. E. Taylor, 2012b: Forcing, feedbacks, and climate sensitivity in CMIP5 coupled atmosphere–ocean climate models. *Geophys. Res. Lett.*, **39**, L09712, doi:10.1029/2012GL051607.
- Barnes, E. A., and L. M. Polvani, 2013: Response of the midlatitude jets and of their variability to increased greenhouse gases in CMIP5 models. *J. Climate*, **26**, 7117–7135, doi:10.1175/JCLI-D-12-00536.1.
- Bender, F. A.-M., V. Ramanathan, and G. Tselioudis, 2012: Changes in extratropical storm track cloudiness 1983–2008: Observational support for a poleward shift. *Climate Dyn.*, **38**, 2037–2053, doi:10.1007/s00382-011-1065-6.

- Bony, S., and J.-L. Dufresne, 2005: Marine boundary layer clouds at the heart of tropical cloud feedback uncertainties in climate models. *Geophys. Res. Lett.*, **32**, L20806, doi:10.1029/2005GL023851.
- Bromwich, D. H., and Coauthors, 2012: Tropospheric clouds in Antarctica. *Rev. Geophys.*, **50**, RG1004, doi:10.1029/2011RG000363.
- Ceppi, P., Y.-T. Hwang, D. M. W. Frierson, and D. L. Hartmann, 2012: Southern Hemisphere jet latitude biases in CMIP5 models linked to shortwave cloud forcing. *Geophys. Res. Lett.*, **39**, L19708, doi:10.1029/2012GL053115.
- , M. D. Zelinka, and D. L. Hartmann, 2014: The response of the Southern Hemisphere eddy-driven jet to future changes in shortwave radiation in CMIP5. *Geophys. Res. Lett.*, **41**, 3244–3250, doi:10.1002/2014GL060043.
- Colman, R. A., and B. J. McAvaney, 2011: On tropospheric adjustment to forcing and climate feedbacks. *Climate Dyn.*, **36**, 1649–1658, doi:10.1007/s00382-011-1067-4.
- Dee, D. P., and Coauthors, 2011: The ERA-Interim reanalysis: Configuration and performance of the data assimilation system. *Quart. J. Roy. Meteor. Soc.*, **137**, 553–597, doi:10.1002/qj.828.
- Dufresne, J.-L., and S. Bony, 2008: An assessment of the primary sources of spread of global warming estimates from coupled atmosphere–ocean models. *J. Climate*, **21**, 5135–5144, doi:10.1175/2008JCLI2239.1.
- Forster, P. M., T. Andrews, P. Good, J. M. Gregory, L. S. Jackson, and M. Zelinka, 2013: Evaluating adjusted forcing and model spread for historical and future scenarios in the CMIP5 generation of climate models. *J. Geophys. Res.*, **118**, 1139–1150, doi:10.1002/jgrd.50174.
- Fyfe, J. C., N. P. Gillett, and F. W. Zwiers, 2013: Overestimated global warming over the past 20 years. *Nat. Climate Change*, **3**, 767–769, doi:10.1038/nclimate1972.
- Gillett, N. P., and D. W. J. Thompson, 2003: Simulation of recent Southern Hemisphere climate change. *Science*, **302**, 273–275, doi:10.1126/science.1087440.
- Gregory, J. M., and Coauthors, 2004: A new method for diagnosing radiative forcing and climate sensitivity. *Geophys. Res. Lett.*, **31**, L03205, doi:10.1029/2003GL018747.
- Grise, K. M., L. M. Polvani, G. Tselioudis, Y. Wu, and M. D. Zelinka, 2013: The ozone hole indirect effect: Cloud-radiative anomalies accompanying the poleward shift of the eddy-driven jet in the Southern Hemisphere. *Geophys. Res. Lett.*, **40**, 3688–3692, doi:10.1002/grl.50675.
- Hwang, Y.-T., and D. M. W. Frierson, 2013: Link between the double-interropical convergence zone problem and cloud biases over the Southern Ocean. *Proc. Natl. Acad. Sci. USA*, **110**, 4935–4940, doi:10.1073/pnas.1213302110.
- Kay, J. E., and Coauthors, 2012: Exposing global cloud biases in the Community Atmosphere Model (CAM) using satellite observations and their corresponding instrument simulators. *J. Climate*, **25**, 5190–5207, doi:10.1175/JCLI-D-11-00469.1.
- , B. Medeiros, Y.-T. Hwang, A. Gettelman, J. Perket, and M. G. Flanner, 2014: Processes controlling Southern Ocean shortwave climate feedbacks in CESM. *Geophys. Res. Lett.*, **41**, 616–622, doi:10.1002/2013GL058315.
- Klein, S. A., Y. Zhang, M. D. Zelinka, R. Pincus, J. Boyle, and P. J. Gleckler, 2013: Are climate model simulations of clouds improving? An evaluation using the ISCCP simulator. *J. Geophys. Res.*, **118**, 1329–1342, doi:10.1002/jgrd.50141.
- Kushner, P. J., I. M. Held, and T. L. Delworth, 2001: Southern Hemisphere atmospheric circulation response to global warming. *J. Climate*, **14**, 2238–2249, doi:10.1175/1520-0442(2001)014<0001:SHACRT>2.0.CO;2.
- Loeb, N. G., S. Kato, W. Su, T. Wong, F. G. Rose, D. R. Doelling, J. R. Norris, and X. Huang, 2012: Advances in understanding top-of-atmosphere radiation variability from satellite observations. *Surv. Geophys.*, **33**, 359–385, doi:10.1007/s10712-012-9175-1.
- Medeiros, B., B. Stevens, I. M. Held, M. Zhao, D. L. Williamson, J. G. Olson, and C. S. Bretherton, 2008: Aquaplanets, climate sensitivity, and low clouds. *J. Climate*, **21**, 4974–4991, doi:10.1175/2008JCLI1995.1.
- Otto, A., and Coauthors, 2013: Energy budget constraints on climate response. *Nat. Geosci.*, **6**, 415–416, doi:10.1038/ngeo1836.
- Pincus, R., S. Platnick, S. A. Ackerman, R. S. Hemler, and R. J. P. Hoffmann, 2012: Reconciling simulated and observed views of clouds: MODIS, ISCCP, and the limits of instrument simulators. *J. Climate*, **25**, 4699–4720, doi:10.1175/JCLI-D-11-00267.1.
- Polvani, L. M., D. W. Waugh, G. J. P. Correa, and S.-W. Son, 2011: Stratospheric ozone depletion: The main driver of twentieth-century atmospheric circulation changes in the Southern Hemisphere. *J. Climate*, **24**, 795–812, doi:10.1175/2010JCLI3772.1.
- Ramanathan, V., R. D. Cess, E. F. Harrison, P. Minnis, B. R. Barkstrom, E. Ahmad, and D. Hartmann, 1989: Cloud-radiative forcing and climate: Results from the Earth Radiation Budget Experiment. *Science*, **243**, 57–63, doi:10.1126/science.243.4887.57.
- Rossow, W. B., and R. A. Schiffer, 1999: Advances in understanding clouds from ISCCP. *Bull. Amer. Meteor. Soc.*, **80**, 2261–2288, doi:10.1175/1520-0477(1999)080<2261:AIUCFI>2.0.CO;2.
- Soden, B. J., and I. M. Held, 2006: An assessment of climate feedbacks in coupled ocean–atmosphere models. *J. Climate*, **19**, 3354–3360, doi:10.1175/JCLI3799.1.
- Son, S. W., and Coauthors, 2008: The impact of stratospheric ozone recovery on the Southern Hemisphere westerly jet. *Science*, **320**, 1486–1489, doi:10.1126/science.1155939.
- Staten, P. W., J. J. Rutz, T. Reichler, and J. Lu, 2012: Breaking down the tropospheric circulation response by forcing. *Climate Dyn.*, **39**, 2361–2375, doi:10.1007/s00382-011-1267-y.
- Stott, P., P. Good, G. Jones, N. Gillett, and E. Hawkins, 2013: The upper end of climate model temperature projections is inconsistent with past warming. *Environ. Res. Lett.*, **8**, 014024, doi:10.1088/1748-9326/8/1/014024.
- Taylor, K. E., R. J. Stouffer, and G. A. Meehl, 2012: An overview of CMIP5 and the experiment design. *Bull. Amer. Meteor. Soc.*, **93**, 485–498, doi:10.1175/BAMS-D-11-00094.1.
- Trenberth, K. E., and J. T. Fasullo, 2010: Simulation of present-day and twenty-first-century energy budgets of the Southern Oceans. *J. Climate*, **23**, 440–454, doi:10.1175/2009JCLI3152.1.
- Tsushima, Y., and Coauthors, 2006: Importance of the mixed-phase cloud distribution in the control climate for assessing the response of clouds to carbon dioxide increase: A multi-model study. *Climate Dyn.*, **27**, 113–126.
- Webb, M. J., and Coauthors, 2006: On the contribution of local feedback mechanisms to the range of climate sensitivity in two GCM ensembles. *Climate Dyn.*, **27**, 17–38, doi:10.1007/s00382-006-0111-2.
- , F. H. Lambert, and J. M. Gregory, 2013: Origins of differences in climate sensitivity, forcing and feedback in climate models. *Climate Dyn.*, **40**, 677–707, doi:10.1007/s00382-012-1336-x.

- Williams, K. D., and M. J. Webb, 2009: A quantitative performance assessment of cloud regimes in climate models. *Climate Dyn.*, **33**, 141–157, doi:[10.1007/s00382-008-0443-1](https://doi.org/10.1007/s00382-008-0443-1).
- Yin, J. H., 2005: A consistent poleward shift of the storm tracks in simulations of 21st century climate. *Geophys. Res. Lett.*, **32**, L18701, doi:[10.1029/2005GL023684](https://doi.org/10.1029/2005GL023684).
- Zelinka, M. D., S. A. Klein, and D. L. Hartmann, 2012: Computing and partitioning cloud feedbacks using cloud property histograms. Part I: Cloud radiative kernels. *J. Climate*, **25**, 3715–3735, doi:[10.1175/JCLI-D-11-00248.1](https://doi.org/10.1175/JCLI-D-11-00248.1).
- , —, K. E. Taylor, T. Andrews, M. J. Webb, J. M. Gregory, and P. M. Forster, 2013: Contributions of different cloud types to feedbacks and rapid adjustments in CMIP5. *J. Climate*, **26**, 5007–5027, doi:[10.1175/JCLI-D-12-00555.1](https://doi.org/10.1175/JCLI-D-12-00555.1).
- Zhang, Y. C., W. B. Rossow, A. A. Lacis, V. Oinas, and M. I. Mishchenko, 2004: Calculation of radiative fluxes from the surface to top of atmosphere based on ISCCP and other global data sets: Refinements of the radiative transfer model and the input data. *J. Geophys. Res.*, **109**, D19105, doi:[10.1029/2003JD004457](https://doi.org/10.1029/2003JD004457).
- Zhang, Y. Y., and Coauthors, 2012: Regional assessment of the parameter-dependent performance of CAM4 in simulating tropical clouds. *Geophys. Res. Lett.*, **39**, L14708, doi:[10.1029/2012GL052184](https://doi.org/10.1029/2012GL052184).